www.sciencemag.org/content/342/6155/235/suppl/DC1

Supplementary Materials for

Antiviral RNA Interference in Mammalian Cells

P. V. Maillard, C. Ciaudo, A. Marchais, Y. Li, F. Jay, S. W. Ding, Olivier Voinnet*

*Corresponding author. E-mail: voinneto@ethz.ch

Published 11 October 2013, *Science* **342**, 235 (2013)
DOI: 10.1126/science.1241930

This PDF file includes

Other Supplementary Material for this manuscript includes the following:
(available at www.sciencemag.org/content/342/6155/235/suppl/DC1)

Table S2. Percentage of total reads obtained from ILLUMINA deep-sequencing analyses.
Reads for all annotated miRNA in mESCs infected or not with EMCV, NoV or NoVΔB2.

Supplementary Text: Author contributions.

OV conceived the primary idea. OV, PVM and CC designed the experiments. PVM, CC, YL and FJ performed the experiments. AM performed all bioinformatics analyses and conceived novel methods for data analyses and presentation. PVM, CC, AM, SWD and OV analyzed the data. PVM and OV wrote the paper.

Materials and Methods

Cell culture and in vitro differentiation of mESCs

mESCs: Female PGK (129xPGK background) (*28*), male HM1 (129/Ola background) (*29*), $Dcr^{Flx/Flx}$ and $Dcr^{-/-}$ (hybrid background) (*30*) were cultured in Dulbecco's Modified Eagle Media (DMEM) (Invitrogen), containing 15% of a special selected batch of fetal bovine serum FBS (Life Technologies) tested for optimal growth of mESCs, 1000 U/mL LIF (Millipore), 0.1 mM 2-β mercaptoethanol (Life Technologies), 0.05 mg/mL of streptomycin (Sigma), and 50 U/mL of penicillin (Sigma) on a gelatin coated support in the absence of feeder cells. Male E14 (129/Ola background) mESC line (*31*) and E14-FHA-hAgo2 (created by the transfection of the plasmid pIRESneo-FLAG/HA Ago2 corrected (Addgene plasmid 10822) (*32*) and selected on G418-containing medium) were cultured in Glasgow MEM medium (Invitrogen), containing 15% FBS (Life Technologies), 1000 U/mL LIF (Chemicon), 0.1 mM 2-β-mercaptoethanol (Invitrogen), 0.05 mg/mL of streptomycin (Invitrogen) and 50 U/mL of penicillin (Invitrogen), 2 mM L-Glutamine, 1 mM Sodium Pyruvate MEM and 1X MEM Amino Acid on a gelatin-coated support in the absence of feeder cells. The culture medium was changed daily. All cells were grown at 37°C in 8% CO_2. New CreERT2-$Dcr^{Flx/Flx}$ mESCs were isolated from the cross of floxed $Dcr^{Flx/Flx}$ mice and ROSA-CreERT2 mice (*30*). Genotyping primers used for the characterization of these cell lines are presented in table S3. The inducible mESC line (E7 line) deficient for the four mouse Argonautes (*Ago1,2,3,4*_KO) and carrying a floxed human *Ago2* transgene was described previously (*33*). *Dcr* and *hAgo2* deletions were induced with 4-OHT (Tam) stock solution (1 mM, dissolved in 100% ethanol) diluted 1:1000 in cell culture medium to a final concentration of 1 µM. To generate $Dcr^{-/-}$, $Dcr^{Flx/Flx}$ mESCs were treated with 4-OHT for 12 days and isolated clones propagated for several passages to obtain

constitutive *Dcr*$^{-/-}$ mESC lines used in our study. Deletion of *Dcr* was verified at the genomic level by genotyping and at the functional level by the loss of production of various miRNAs (miR-295, miR-16) as well as the increased abundance of known targets of miRNAs (Hmga2 and Btg2). Embryoid body cultures were established by aggregation of mESCs in a low-adherent tissue culture dish into LIF-free DMEM, 10% FBS medium until day 10 of differentiation. The culture medium was changed daily. All cells were grown at 37°C in 8% CO_2. BHK-21 cells (a kind gift of Gisou Van der Goot) were cultivated in Dulbecco's modified Eagle with Glutamax™ medium (Gibco, Life Technologies) supplemented with 10% fetal bovine serum "Gold" (PAA), 100 U/mL penicillin (Sigma) and 0.1 mg/mL streptomycin (Sigma).

Production of recombinant virus

EMCV was produced as described (*34*) using the recombinant vector containing the full-length cDNA clone (pBL/T7EMCgB2887) of an EMCV strain (2887A/91) kindly provided by L. Bakkali-Kassimi (ANSES, Maisons-Alfort, France). Briefly, pBL/T7EMCgB2887 (10 µg) was linearized with *Not I* for 4 hours and DNA purified using GeneJET Gel Extraction and DNA Cleanup Micro Kit (Fermentas). *In vitro* transcription was performed with T7 RNA polymerase on the linearized plasmid (1 µg) at 37°C for 2 hours using the MEGAscript kit (Ambion). DNA was then digested by Turbo™ DNAse (Ambion) for 30 min at 37°C and RNA extracted with Tri-Reagent (Sigma) according the manufacturer's instructions. The size of the synthesized RNA was determined on formaldehyde agarose electrophoresis. *In vitro* transcribed RNA (4 µg) was transfected in 50% confluent BHK-21 cells in a six-well culture dish, using 3:1 ratios of FuGENE 6 (Roche Applied Science) transfection reagent (µL) to DNA (µg), respectively. Two days later, when cytopathic effect (CPE) was apparent, supernatant was harvested and clarified by centrifugation (1500 rpm/ 300 g, 5 min). The rescued virus was passaged on BHK-21 cells by infecting 50% confluent cells in T75 Flask with 1mL EMCV-containing supernatant and cells incubated for 1 hour at 37°C in 5% CO_2. Then culture medium was added and cells incubated for one day until appearance of CPE. Cells were then lysed by 3 freeze-thaw cycles and supernatants subsequently collected, clarified by centrifugation (1500 rpm/ 300 g, 5 min), aliquoted and stored at -80°C. Titers

were determined by 50% Tissue Culture Infective Dose ($TCID_{50}$) assays on BHK-21 cells. Briefly, BHK-21 cells were infected with 10-fold dilutions of the virus and incubated at 37°C in 5% CO_2 for one to two days. CPE was determined by inspection under the microscope and the numbers of wells with CPE used to calculate $TCID_{50}$ using Reed and Muench statistical method. NoV and NoVΔB2 DNA clones and virion production were as described in the accompanying paper (*23*).

Infections of mESCs

Infections with EMCV: At the day of infection, the medium was changed and EMCV added at a dose (determined in BHK-21 cells) of 50-100 $TCID_{50}$/cell on 50-80% confluent mESCs cultured in T75 flasks. Cells were incubated for 3 or 6 hours post-infection at 37°C in 8% CO_2 and then washed twice with phosphate buffered-saline 1X (PBS1X), trypsinized and then collected. Cells were pelleted, washed one more time with PBS1X and processed for downstream applications. For experiments aimed at testing the DCR-dependency of EMCV-derived small RNAs we used $Dcr^{Flx/Flx}$ and constitutive $Dcr^{-/-}$ mESCs maintained in culture over multiple passages and seeded in T-75 flasks one day before the infection. The density was such that a similar number of $Dcr^{Flx/Flx}$ and $Dcr^{-/-}$ mESCs was attained on the day of infection. Cells were then challenged with EMCV following the aforementioned procedure for infection.

Infections with NoV and NoV ΔB2: At the day of infection, a mix was prepared in which virus preparations (1 mL of NoV or 1 mL of NoVΔB2) were mixed with FBS-free Glasgow MEM complete medium (9 mL). E14 mESC line grown in T75 flasks at a confluency of 30-40% were washed twice with Dulbecco's Phosphate-Buffered Saline (DPBS) containing calcium and magnesium (Gibco, Life Technologies) and then infected by addition of the infection mix. Cells were incubated for 1 hour at 37°C in 8% CO_2 and then medium was changed and cells incubated for 3 days at 37°C in 8% CO_2. Cells were then washed with PBS1X without calcium and magnesium (Gibco, Life Technologies), trypsinized and pelleted for downstream applications. For the genetic rescue experiment, infections were conducted on the inducible mESC line (E7 line) deficient for the four mouse Argonautes (*Ago1,2,3,4*_KO) and carrying a floxed human *Ago2* transgene (*33*).

Before infection, the E7 mESC line was treated with 4-OHT (used at 1 μM) for 2 days to induce the deletion of the *Ago2* transgene, while untreated E7 mESCs were used a control. Two days later, untreated and treated E7 mESCs were challenged with NoV or NoVΔB2 following the aforementioned procedure of infection. Cells were then incubated in the presence of 4-OHT for a further 3 days at 37°C in 8% CO_2, washed with PBS1X without calcium and magnesium, and pelleted for downstream applications.

Deep-Sequencing and sRNA analyses

Total RNA was extracted using Isol-RNA Lysis Reagent (5PRIME) and 5 μg processed into sequencing libraries using adapted Illumina protocols for Illumina technology and sequenced by Fasteris SME (http://www.fasteris.com, Switzerland). All next-generation sequencing data have been submitted to the NCBI Gene Expression Omnibus (GEO) and are accessible with the accession number GSE43153. The ncPRO pipeline (*35*) was used to filter out the reads mapping against the mouse genome and to analyze globally the quality of deep-sequencing. The reads not matching the mouse genome were mapped against the viral genomes using Bowtie (*36*) with the default options: but –m 5000 and –e 50. The EMCV and two NoV genome sequences with the respective reference names, AF356822.1, NC_002690.1 and NC_002691.1, have been downloaded from the NCBI ftp repository (http://www.ncbi.nlm.nih.gov/Ftp/). For all phasing/periodicity studies, the read counts were calculated based on either:

- The 5'-end coordinates for the reads produced from the (+) strand and the 3'-end coordinates for the reads produced from the (-) strand.

- Or, conversely, the 3'-end coordinates for the reads produced from the (+) strand and the 5'-end coordinates for the reads produced from the (-) strand (data not shown).

The radar plots represent the phasing by displaying the abundance of reads falling into each of 22 possible registers. The register abundance calculations were computed as the frequency of the modulo-22 of the coordinate of each read mapping the viral genomes. The registers and the histograms displaying the reads were generated using in-house R-cran scripts (*37*). Auto-correlation is a well-established mathematical tool to detect repeated patterns. This method displays the correlation of a variable (here

abundance of reads along the entire viral genome) against itself. Applied with an increasing lag from 1-nt to 100-nt it allowed detection of periodicity (phasing) in the reads mapping the viral genomes even when the 5' end peaks of 21-to-23-nt reads were omitted form the data set. P-values were calculated using a Pearson correlation test. The harmonic model signal reconstruction is based on a singular spectrum analysis used classically for signal periodicity analysis or forecasting in climatology (*38*). We applied this methodology by considering the abundance of reads along the viral genome as a signal. After a first step of signal decomposition on the first 300-nt in eigenvectors using a window parameter set at 110-nt for EMCV and NoV, a model signal was reconstructed for each strand using the 10 best eigenvectors i.e the best contributors to the total variance. This allowed noise removal and reconstruction of the signal fitting the main trends of the raw data. For enhanced clarity, the model signal levels were multiplied by five. The auto-correlation was calculated considering only the 21-to-23 nt reads whereas the singular spectrum analysis included all reads. The auto-correlation and the singular spectrum analyses were conducted with the Rssa package in R (*39*).

Protein analyses

Total proteins were extracted in a radioimmune precipitation assay (RIPA) buffer (Phosphate Buffered-Saline (PBS) with 1% NP-40, 0.5% sodium deoxycholate and 0.1% SDS) supplemented with Protease Inhibitor Cocktail (Complete, Roche). Protein were quantified using the Bio-Rad *DC* Protein assay kit and equal amounts of protein were resolved on a Tris-glycine SDS-Polyacrylamide gel, transferred by electroblotting onto Inmobilon-P PVDF membrane (Millipore) and incubated with antibodies in PBS with 0.2% Tween-20 and 5% non-fat dried milk following standard Western blot procedures (*40*). After incubation with HRP-conjugated secondary antibody, signal was revealed using the ECL Western Blotting Detection Kit (GE Healthcare). The capsid protein VP1 from EMCV was detected using the mouse monoclonal anti-VP1 antibody (purchased from Dr. Emiliana Brocchi's laboratory, Brescia, Italy). The endogenous mouse AGO2 and OCT4 proteins were detected using the rat anti-mouse Ago2 (clone 6F4, gift of Dr Gunter Meister, University of Regensburg, Germany) and the rabbit anti-Oct4 (ab19857, Abcam, Cambridge, UK) antibodies, respectively. HA-tagged proteins were detected

using peroxydase-conjugated rat monoclonal antibody (clone 3F10, Roche). ACTIN protein was used as a protein loading control and was detected using an anti-actin mouse monoclonal antibody (Chemicon). Alternatively, equal loading was verified by Coomassie staining of the membrane after Western blotting.

RNA analyses

Total RNA from mESCs and from 3 weeks-old seedlings of *Arabidopsis thaliana* SUC:*SUL* line (ecotype Col-0) (*41*) were extracted and purified using Isol-RNA Lysis Reagent (5PRIME) according to manufacturer's instructions. For Northern blot analysis of low molecular weight (LMW) RNA, total RNA was fractionated and LMW RNA isolated as described (*42*). The yield was determined using a spectrophotometer and equal amounts of LMW RNA (2-10 μg) were resolved on denaturing 17.5% polyacrylamide/urea gels, transferred on a Hybond™-NX membrane (GE Healthcare) and chemically cross-linked using 1-ethyl-3-(3-dimethylaminopropyl) carbodiimide (EDC) as previously described (*43*). For Northern blot analysis of high molecular weight (HMW) RNA, 5 μg of total RNA was resolved on denaturing 1.2% agarose gels with 2.2 M formaldehyde, capillary transferred to Hybond™-NX membrane (GE Healthcare) and cross-linked by UV irradiation (*40*). Equal loading was verified before transfer by ethidium bromide staining of total RNA within the RNA gel. Perfect-Hyb buffer (Sigma) was used for the hybridization step in both LMW and HMW Northern blot. DNA oligonucleotides complementary to miR-16 or U6 and locked nucleic acid (LNA™, Exiqon) complementary to EMCV (+) viRNAs were 5'end-labeled with [γ^{32}P]ATP using T4 Polynucleotide Kinase (Thermo Scientific). The probe used to detect SUL siRNAs was made by random priming in the presence of α-32P-dCTP (Hartmann Analytic) using the Prime-a-gene kit (Promega). The template used for this random priming reaction was a 400-bp long PCR product amplified from Arabidopsis genomic DNA (ecotype Col-0) using SUL_Fwd and SUL_Rev primers (table S3). All probes used for Northern blot in this study are listed in table S3.

PCR

Real-time PCR were performed as described (*42*). Briefly, Real-time PCR reagents for miRNAs and control U6 snRNA were from Qiagen. For RT reactions, 1 µg total RNA was reverse transcribed using the miScript Reverse Transcription Kit (Qiagen) following the manufacturer's instructions. Following the RT reactions, cDNA products were diluted five times in distilled water, and 2 µL of the diluted cDNAs was used for PCR using QuantiTect SYBR Green PCR Master Mix and miScript Universal Primer (Qiagen). PCR reactions were conducted at 95°C for 10 min, followed by 40 cycles at 95°C for 15 s and 60°C for 30 s on a LightCycler 480 real-time PCR machine (Roche). Real-time PCR for mRNAs was performed as described in (*44*) using the Rrm2 as a reporter gene. Differences between samples and controls were calculated based on the $2^{-\Delta CT}$ method. Each Real-time PCR reaction was carried out in triplicates using samples from two independent cultures of all mESCs. All the primers used in this study are listed on table S3.

Cell lysates and Immunoprecipitations

mESCs were scraped in cell lysis buffer (25 mM Tris, pH 7.9, 250 mM KCl, 0.2 mM EDTA, 20% glycerol supplemented with Protease Inhibitor Cocktail (Complete, Roche). Cells were lysed 10 min on ice, sonicated, and centrifuged (10 000 rpm, 10 min at 4°C) before Western blot or immunoprecipitation (IP). For E14-FHA-hAgo2, lysates were incubated at 4°C with 20 µL of anti-FLAG-magnetic-beads (Invitrogen) for 12 h. For IP of the endogenous mAGO2, E14 lysates were incubated at 4°C with 20 µL of G-agarose-beads (Invitrogen) for 2 h and then overnight with 1/10 rat anti-mouse Ago2 antibody (clone 6F4, gift of Dr. Gunter Meister, University of Regensburg, Germany). The next day, lysates were incubated again at 4°C with 20 µL of G-agarose-beads (Invitrogen) for 2 h. Beads were collected by centrifugation (2 000 rpm, 1 min). For IP of E14-FHA-hAGO2, at least three washes in 1 mL lysis buffer were performed and beads incubated with 100 µL 0.1 M glycine pH 2.5 for 10 min RT on a shaker. Ten µL 1 M Tris–HCl pH 8 was added to neutralize the elution buffer. Immunoprecipitated RNAs have been extracted from eluted proteins with Isol-RNA Lysis Reagent (5PRIME). For the IP of endogenous mAGO2, beads were washed three times, resuspended in 1 mL Isol-RNA

Lysis Reagent (5PRIME). RNA was isolated following manufacturer's instructions and proteins were precipitated from the phenol phase by addition of 5 volume of ice-cold acetone and incubated at -20°C overnight. After 15 min centrifugation at 13 500 rpm at 4°C, the precipitate was washed with ice-cold 80% acetone and resuspended in a buffer containing 3% [v/v] SDS, 62.3 mM Tris-HCl pH 8, 10% [v/v] glycerol.

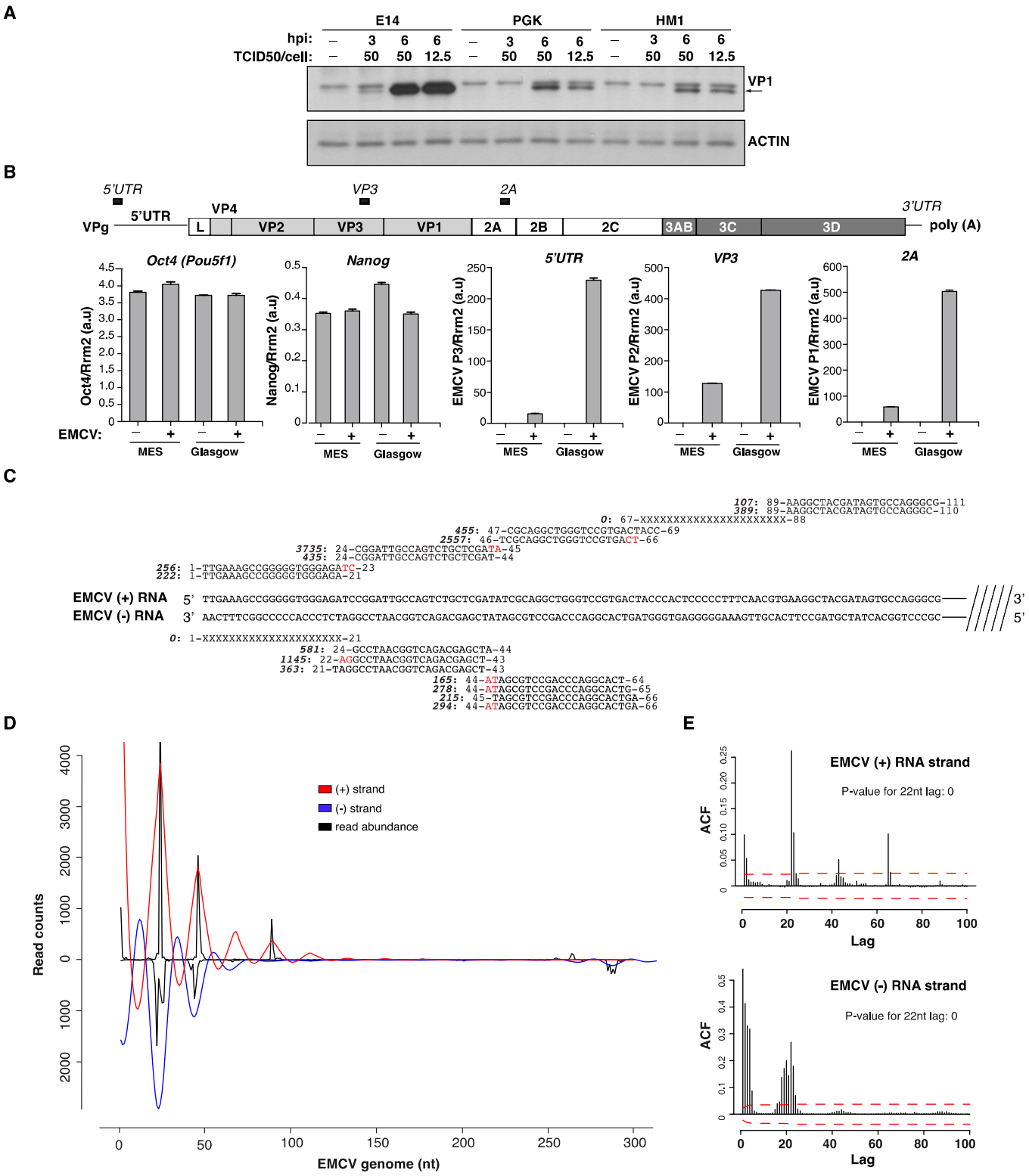
A
E14
PGK
HM1
hpi: – 3 6 6 – 3 6 6 – 3 6 6
TCID50/cell: – 50 50 12.5 – 50 50 12.5 – 50 50 12.5
VP1
ACTIN
B
5'UTR
VP3
2A
3'UTR
VPg
5'UTR
VP4
L
VP2
VP3
VP1
2A
2B
2C
3AB
3C
3D
poly (A)
Oct4 (Pou5f1)
Oct4/Rrm2 (a.u)
Nanog
Nanog/Rrm2 (a.u)
5'UTR
EMCV P3/Rrm2 (a.u)
VP3
EMCV P2/Rrm2 (a.u)
2A
EMCV P1/Rrm2 (a.u)
EMCV:
MES
Glasgow
C
107: 89-AAGGCTACGATAGTGCCAGGGCG-111
389: 89-AAGGCTACGATAGTGCCAGGGC-110
0: 67-XXXXXXXXXXXXXXXXXXXXXX-88
455: 47-CGCAGGCTGGGTCCGTGACTACC-69
2557: 46-TCGCAGGCTGGGTCCGTGACT-66
3735: 24-CGGATTGCCAGTCTGCTCGAATA-45
435: 24-CGGATTGCCAGTCTGCTCGAT-44
256: 1-TTGAAAGCCGGGGGTGGGAGATC-23
222: 1-TTGAAAGCCGGGGGTGGGAGA-21
EMCV (+) RNA 5' TTGAAAGCCGGGGGTGGGAGATCCGGATTGCCAGTCTGCTCGATATCGCAGGCTGGGTCCGTGACTACCCACTCCCCCTTTCAACGTGAAGGCTACGATAGTGCCAGGGCG 3'
EMCV (-) RNA 3' AACTTTCGGCCCCCACCCTCTAGGCCTAACGGTCAGACGAGCTATAGCGTCCGACCCAGGCACTGATGGGTGAGGGGGAAAGTTGCACTTCCGATGCTATCACGGTCCCGC 5'
0: 1-XXXXXXXXXXXXXXXXXXXXX-21
581: 24-GCCTAACGGTCAGACGAGCTA-44
1145: 22-AGGCCTAACGGTCAGACGAGCT-43
363: 21-TAGGCCTAACGGTCAGACGAGCT-43
165: 44-ATAGCGTCCGACCCAGGCACT-64
278: 44-ATAGCGTCCGACCCAGGCACTG-65
215: 45-TAGCGTCCGACCCAGGCACTGA-66
294: 44-ATAGCGTCCGACCCAGGCACTGA-66
D
Read counts
(+) strand
(-) strand
read abundance
EMCV genome (nt)
E
EMCV (+) RNA strand
P-value for 22nt lag: 0
ACF
Lag
EMCV (-) RNA strand
P-value for 22nt lag: 0
ACF
Lag

Fig. S1

Fig. S1.

(**A**) Western analysis of EMCV viral protein 1 (VP1) in various mESC lines (E14, PGK, HM1) in non-infected (-) or at 3 hours or 6 hours post-infection (hpi) with the indicated virus titer determined on BHK-21 cells. $TCID_{50}$/cell: 50% tissue culture infective dose per cell. (**B**) Schematic representation of the EMCV genome (top) and quantitative real-time PCR analysis (qRT-PCR) (bottom) of pluripotency factors Oct4, Nanog and EMCV RNA (5'UTR, VP3 and 2A) in mESCs infected (+) or not (-) in ES or Glasgow media. Positions of the 3 pairs of primers used to quantify EMCV RNA by qRT-PCR analysis are indicated with black bars on the EMCV genome map. Results are mean and standard deviations (SD) of two independent experiments. (**C**) Sequences of reads 21-23-nt along the first 5'-terminal 110-nt of the EMCV RNA (+) and (-) strands. For each sequence the corresponding number of reads (in bold italic) with its position (in nt) along the viral genome and its sequenced variants are indicated. Read sequences not detected by deep-sequencing are depicted with each nucleotide symbolised by X and assembled following the apparent phased production of viRNAs with the ~22-nt periodicity. The 2-nt 3' overhangs are represented in red. (**D**) Model periodic signals reconstructed by a singular spectrum analysis from the 10 top contributors to the total variance extracted from the raw data by a singular spectrum analysis (see methods). The model periodic signals for the 5'-end reads of the EMCV RNA (+) strand and the 3'-end reads for the (-) strand are indicated by red and blue lines, respectively. Corresponding raw count for (+) and (-) strands are indicated with a black line. (**E**) Auto-correlation plot displaying the periodicity of the 5'-end reads of the EMCV RNA (+) strand and of the 3'-end reads for the (-) strand. Confidence interval of 0.95 is indicated with red dashed lines. ACF: auto-correlation function.

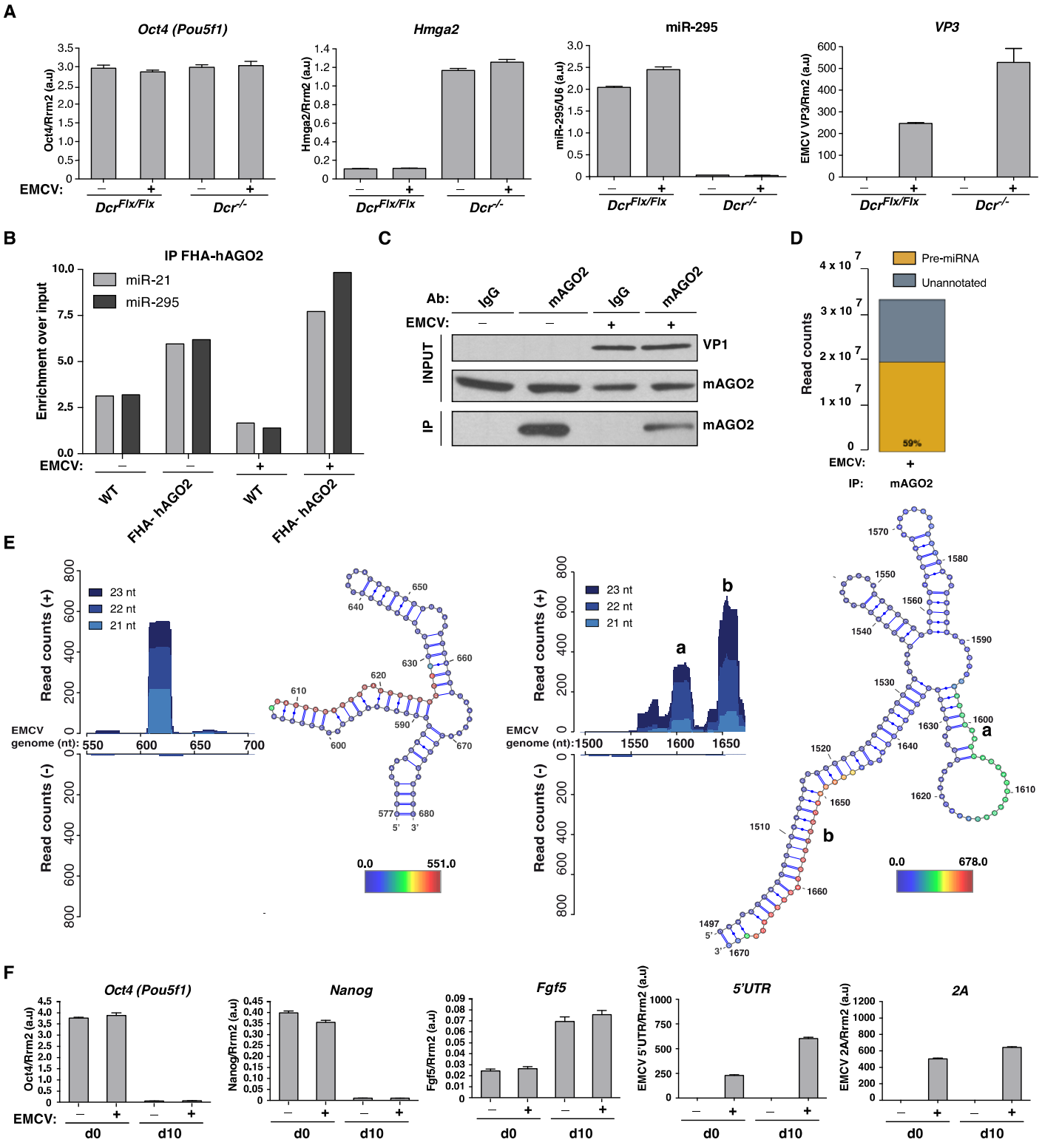
A
Oct4 (Pou5f1)
Hmga2
miR-295
VP3
Oct4/Rrm2 (a.u)
Hmga2/Rrm2 (a.u)
miR-295/U6 (a.u)
EMCV VP3/Rrm2 (a.u)
EMCV:
Dcr Flx/Flx
Dcr -/-
B
IP FHA-hAGO2
miR-21
miR-295
Enrichment over input
EMCV:
WT
FHA-hAGO2
C
Ab:
IgG
mAGO2
INPUT
IP
VP1
mAGO2
D
Pre-miRNA
Unannotated
Read counts
59%
IP:
mAGO2
E
23 nt
22 nt
21 nt
Read counts (+)
Read counts (-)
EMCV genome (nt):
0.0
551.0
678.0
F
Oct4 (Pou5f1)
Nanog
Fgf5
5'UTR
2A
Oct4/Rrm2 (a.u)
Nanog/Rrm2 (a.u)
Fgf5/Rrm2 (a.u)
EMCV 5'UTR/Rrm2 (a.u)
EMCV 2A/Rrm2 (a.u)
d0
d10

Fig. S2

Fig. S2

(**A**) qRT-PCR analyses of the Oct4 mRNA, of one established mESC miRNA target (Hmga2 regulated by miR-196a), of miR-295 and of the EMCV RNA (VP3 region) in $Dcr^{Flx/Flx}$ and $Dcr^{-/-}$ mESCs infected (+) or not (-) with EMCV. Results are mean and standard deviations (SD) of two independent experiments. (**B**) Enrichment of miR-21 and miR-295 in FLAG-specific immunoprecipitation (IP FLAG) in WT mESCs or mESCs stably expressing epitope-tagged FLAG-HA human AGO2 (FHA-hAGO2) infected (+) or not (-) with EMCV, assessed by qRT-PCR analysis. SD calculated from qRT-PCR carried out in triplicates. (**C**) Immunoprecipitation of endogenous mouse AGO2 (mAGO2) using specific antibody or IgG control (IgG) in mESCs infected (+) or not (-) with EMCV. Protein blot analysis ensures comparable levels of infection (VP1, top) and confirms mAGO2 immunoprecipitation (bottom). (**D**) Percentage of reads mapping to pre-miRNA in IP of endogenous mAGO2 (mAGO2) of EMCV-infected mESCs shown in (C), as annotated by the ncPRO pipeline. Reads are classified as "unannotated" when they do not map any pre-miRNA. (**E**) 21-23-nt read distribution along the EMCV genome upon deep-sequencing of RNA isolated from endogenous AGO2 IP 6 hpi of mESCs. The two regions depicted correspond to the peaks marked with asterisks in the main Fig. 2C. The panel on the left depicts the J-motif of the EMCV IRES, the structure of which has been previously validated by nuclease probing (*45*); it is noteworthy that the major small RNA species corresponds to the binding site of EiF4A, known to change the IRES local confirmation (*46*). The RNA structure (*47*) on the right panel was predicted by RNA fold (*48*) but not validated experimentally. The two peaks (a and b) present in the EMCV genome at nt 1497-1670 are depicted on the corresponding RNA structure. The most abundant reads are indicated in red within the structures, and heat maps representing read variants or secondary reads. (**F**) qRT-PCR analysis of Oct4 and Nanog (pluripotency markers) and Fgf5 (ectoderm marker) in mESCs at day 0 (d0) and at day 10 (d10) of differentiation, infected (+) or not (-) with EMCV. Parallel quantification of EMCV RNA accumulation by qRT-PCR, as in fig.S1B, is presented in the two rightmost panels (5'UTR and 2A). Results are mean and SD of two independent experiments.

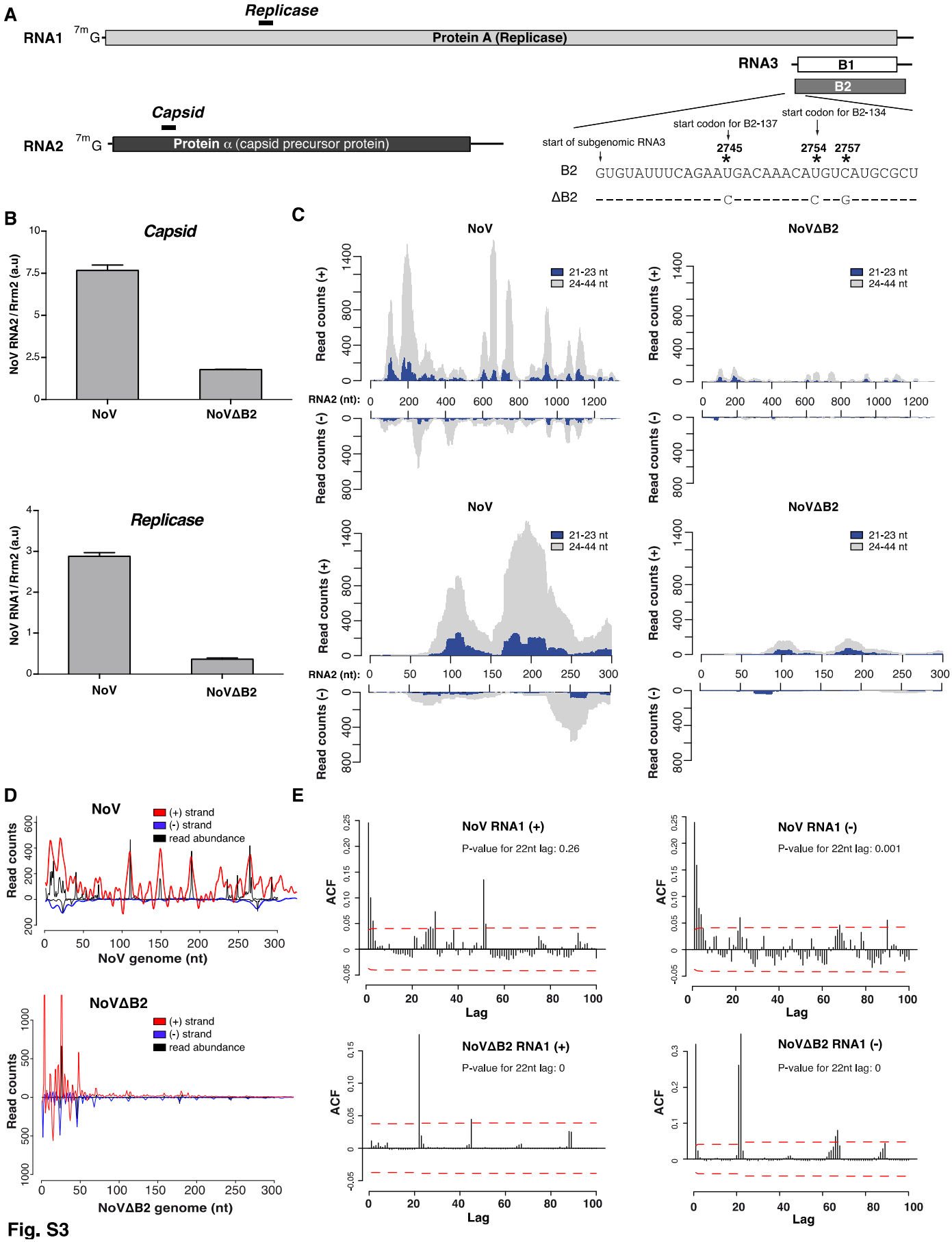
A
Replicase
RNA1
7m G
Protein A (Replicase)
RNA3
B1
B2
Capsid
RNA2
7m G
Protein α (capsid precursor protein)
start codon for B2-137
start codon for B2-134
start of subgenomic RNA3
2745
2754
2757
B2 GUGUAUUUCAGAAUGACAAACAUGUCAUGCGCU
ΔB2 ----------C--------C--G-------
B
Capsid
NoV RNA2/Rrm2 (a.u)
NoV
NoVΔB2
Replicase
NoV RNA1/Rrm2 (a.u)
C
NoV
NoVΔB2
Read counts (+)
Read counts (-)
21-23 nt
24-44 nt
RNA2 (nt):
D
NoV
(+) strand
(-) strand
read abundance
Read counts
NoV genome (nt)
NoVΔB2
NoVΔB2 genome (nt)
E
NoV RNA1 (+)
P-value for 22nt lag: 0.26
NoV RNA1 (-)
P-value for 22nt lag: 0.001
NoVΔB2 RNA1 (+)
P-value for 22nt lag: 0
NoVΔB2 RNA1 (-)
P-value for 22nt lag: 0
ACF
Lag

Fig. S3

Fig. S3

(**A**) Schematic representation of the two NoV genomic (RNA1 and RNA2) and single subgenomic RNA (RNA3, from which the B2 protein is produced). The mutations engineered in RNA1 to create NoVΔB2 are depicted: U2745C and U2754C disrupt the start codons of both *B2* open reading frames (*B2-137* and *B2-134)*, while C2757G generates a stop codon. None of these 3 mutations affects the overlapping Protein A/B1 ORF. The absence of B2 production from NoVΔB2 was confirmed by Li *et al*. in the accompanying manuscript (*23*). The positions of the oligonucleotide primers used in (B) for qRT-PCR analysis are indicated with black bars. (**B**) Quantification of *Replicase* (left) and *Capsid* (right) by qRT-PCR analysis in mESCs infected with NoV or NoVΔB2. Results are mean and SD of two independent experiments. (**C**) Same as in main Fig. 3C, but with deep-sequencing reads mapping to the RNA2 of NoV and NoVΔB2. (**D**) Same as in Fig. S1D, but with deep-sequencing reads mapping to the RNA1 of NoV and NoVΔB2. (**E**) Same as in Fig. S1E, but with deep-sequencing reads mapping to the RNA1 of NoV and NoVΔB2.

Table S1.

Quantitative data from ILLUMINA deep-sequencing analyses

Mapped target region / size of reads mapped	Read characteristics	infections with EMCV					infections with NoV		infections with NoVΔB2	
		mESCs d0			mESCs d10	IP mAGO2	RNA1	RNA2	RNA1	RNA2
		3 hpi	6 hpi	6 hpi	6 hpi	6 hpi	72 hpi	72 hpi	72 hpi	72 hpi
	Total mapped reads	33,989,187	28,024,435	30,159,934	28,032,772	36,841,148	42,698,984	42,633,218	35,994,680	35,982,151
	mapped	33,985,104	27,903,177	29,945,086	27,991,320	36,682,302	42,616,920	42,616,920	35,980,340	35,980,340
	21-nt	3,507,409	3,210,403	3,523,909	2,732,889	3,476,292	4,412,863	3,886,312	4,412,863	3,886,312
mouse genome/ 19-44-nt	22-nt	8,722,629	8,104,811	7,692,901	7,030,673	7,541,514	10,584,482	10,275,923	10,584,482	10,275,923
	23-nt	5,318,723	3,991,681	4,615,584	4,771,356	4,993,130	5,839,149	5,299,375	5,839,149	5,299,375
	Total 21-23-nt	17,548,761	15,306,895	15,832,394	14,534,918	16,010,936	20,836,494	19,461,610	20,836,494	19,461,610
	miRNAs	22,338,674	13,719,791	18,833,978	16,337,825	26,047,613	21,653,457	21,653,457	17,533,962	17,533,962
	% of mouse mapped miRNAs	65.73	49.17	62.90	58.37	71.01	50.81	50.81	48.73	48.73
	mapped	4,083	121,258	214,848	41,452	158,846	82,064	16,298	14,340	1,811
	mapped on the (+) strand	3,905	110,311	197,877	40,325	155,477	69,411	12,689	10,217	1,476
	mapped on the (-) strand	178	10,947	16,971	1,127	3,369	12,653	3,612	4,123	335
viral genome / 19-44-nt	(+):(-) strand ratio	21.9	10.1	11.7	35.8	46.1	5.5	3.5	2.5	4.4
	unique sequence	1,230	13,088	28,480	11,489	12,896	15,479	4,497	4,731	923
	% of total reads	0.01	0.43	0.71	0.15	0.43	0.19	0.04	0.04	0.01
	mapped	179	17,011	18,383	2,455	3,632	4,851	2,805	2,635	487
	mapped on the (+) strand	169	10,971	11,403	2,310	2,290	4,311	2,435	1,987	401
	mapped on the (-) strand	10	6,040	6,980	145	1,342	540	370	648	86
viral 5' terminal 200-nt region/ 19-44-nt	(+):(-) strand ratio	16.9	1.8	1.6	15.9	1.7	8.0	6.6	3.1	4.7
	unique sequence	29	229	336	120	121	714	745	286	217
	% of total reads	0.00	0.06	0.06	0.01	0.01	0.01	0.01	0.01	0.00
	mapped	789	39,917	58,665	6,780	18,574	12,648	2,323	6,596	454
	mapped on the (+) strand	712	31,003	44,381	6,392	16,231	10,398	1,761	4,061	314
	mapped on the (-) strand	77	8,914	14,284	388	2,343	2,250	563	2,535	140
viral genome/ 21-23-nt	(+):(-) strand ratio	9.2	3.5	3.1	16.5	6.9	4.6	3.1	1.6	2.2
	unique sequence	229	2,802	5,449	1,665	1,596	2,403	660	1,408	215
	% of total reads	0.00	0.14	0.19	0.02	0.05	0.03	0.01	0.02	0.00
	% of mouse mapped 21-23-nt reads	0.00	0.26	0.37	0.05	0.12	0.06	0.01	0.03	0.00
	mapped	65	14,212	16,186	695	2,160	653	467	2,068	181
	mapped on the (+) strand	55	9,288	10,016	578	995	560	374	1,523	112
	mapped on the (-) strand	10	4,924	6,170	117	1,205	93	93	545	69
viral 5' terminal 200-nt region/ 21-23-nt	(+):(-) strand ratio	5.5	1.9	1.6	4.9	0.8	6.0	4.0	2.8	1.6
	unique sequence	12	113	161	40	58	115	119	93	61
	% of total reads	0.00	0.05	0.05	0.00	0.01	0.00	0.00	0.01	0.00
	% of mouse mapped 21-23-nt reads	0.00	0.09	0.10	0.00	0.01	0.00	0.00	0.01	0.00

hpi : hours post-infection

Table S3.

Primer sequences

Probes for Northern analysis

Description	sequence 5' to 3'
miR-16	GCCAATATTTACGTGCTGCTA
U6	GCAGGGGCCATGCTAATCTTCTCTGTATCG
EMCV (+) viRNA	TATCGAGCAGACTGGCAATCCG (LNA™ probe from Exiqon)
NoV RNA1 and RNA3	ATCGTTGCTTGCGTCTCCTGAGCCAGCTGCTCCAGCTTGG
SUL_Fwd	ATATCGAAAAGGCTTTGACAGAAG
SUL_Rev	AATCTGGTCTTGAAGCTTGTCC

Primers for qRT-PCR on viral RNA and cellular mRNA

Description	sequence 5' to 3'
EMCV 2A_Fwd	AGGCGGTTCTAAGAGCAGAACCAT
EMCV 2A_Rev	AGTGGGCATTGAAGATCCGGTACA
EMCV VP3_Fwd	CCATGCAGGCGACTTATGCGATTT
EMCV VP3_ Rev	TAACCCAGCCATCCGCATTAGTGA
EMCV 5'UTR_Fwd	TTGAAAGCCGGGGGTGGGAGATCC
EMCV 5'UTR_Rev	GTTTGTTGTTGTTTTGGGGTGGC
NoV Replicase_Fwd	CCGTTCATGGCTTACACCTT
NoV Replicase_Fwd	GCACCAGTCCCAAACTTCAT
NoV Capsid_Fwd	CAGAGAATGGCAGCAACAAA
NoV Capsid_Rev	CGGTAAAACGAGACCCTGAA
Rrm2_Fwd	CCGAGTCGGAAAGTAAAGCG
Rrm2_Rev	ATGGGAAAGACAACGAAGCG

Btg2_Fwd	GCGAGCAGAGACTCAAGGTT
Btg2_Rev	TAGCCAGAACCTTTGGATGG
Pou5f1_Fwd (Oct4)	CAACTCCCGAGGAGTCCCA
Pou5f1_Rev (Oct4)	CTGGGTGTACCCCAAGGTGA
Nanog_Fwd	CAGAAAAACCAGTGGTTGAAGACTAG
Nanog_Rev	GCAATGGATGCTGGGATACTC
Fgf5_Fwd	TGTACTGCAGAGTGGGCATC
Fgf5_Rev	ACAATCCCCTGAGACACAGC

Primers for qRT-PCR on miRNAs and U6 snRNA

Description	**sequence 5' to 3'**
U6	Hs_RNU6-2_1 (Qiagen)
miR-295	AAAGUGCUACUACUUUUGAGUCU
miR-21	UAGCUUAUCAGACUGAUGUUGA

Primers for genotyping

Description	**sequence 5' to 3'**
DICER 460 R	GTACGTCTACAATTGTCTATG
DICER 23 F	ATTGTTACCAGCGCTTAGAATTCC
DICER 458 F	TCGGAATAGGAACTTCGTTAAAC

Additional Data table S2 (separate file)

Percentage of total reads obtained from ILLUMINA deep-sequencing analyses for all annotated miRNA in mESCs infected or not with EMCV, NoV or NoVΔB2.

References

1. J. Haasnoot, E. M. Westerhout, B. Berkhout, RNA interference against viruses: Strike and counterstrike. *Nat. Biotechnol.* **25**, 1435–1443 (2007). Medline doi:10.1038/nbt1369

2. J. L. Umbach, B. R. Cullen, The role of RNAi and microRNAs in animal virus replication and antiviral immunity. *Genes Dev.* **23**, 1151–1164 (2009). Medline doi:10.1101/gad.1793309

3. D. Goubau, S. Deddouche, C. Reis E Sousa, Cytosolic sensing of viruses. *Immunity* **38**, 855–869 (2013). Medline doi:10.1016/j.immuni.2013.05.007

4. K. Chalupnikova, J. Nejepinska, P. Svoboda, Production and application of long dsRNA in mammalian cells. *Methods Mol. Biol.* **942**, 291–314 (2013). Medline doi:10.1007/978-1-62703-119-6_16

5. P. Parameswaran, E. Sklan, C. Wilkins, T. Burgon, M. A. Samuel, R. Lu, K. M. Ansel, V. Heissmeyer, S. Einav, W. Jackson, T. Doukas, S. Paranjape, C. Polacek, F. B. dos Santos, R. Jalili, F. Babrzadeh, B. Gharizadeh, D. Grimm, M. Kay, S. Koike, P. Sarnow, M. Ronaghi, S. W. Ding, E. Harris, M. Chow, M. S. Diamond, K. Kirkegaard, J. S. Glenn, A. Z. Fire, Six RNA viruses and forty-one hosts: Viral small RNAs and modulation of small RNA repertoires in vertebrate and invertebrate systems. *PLoS Pathog.* **6**, e1000764 (2010). Medline doi:10.1371/journal.ppat.1000764

6. R. Aliyari, Q. Wu, H. W. Li, X. H. Wang, F. Li, L. D. Green, C. S. Han, W. X. Li, S. W. Ding, Mechanism of induction and suppression of antiviral immunity directed by virus-derived small RNAs in *Drosophila*. *Cell Host Microbe* **4**, 387–397 (2008). Medline doi:10.1016/j.chom.2008.09.001

7. A. Deleris, J. Gallego-Bartolome, J. Bao, K. D. Kasschau, J. C. Carrington, O. Voinnet, Hierarchical action and inhibition of plant Dicer-like proteins in antiviral defense. *Science* **313**, 68–71 (2006). Medline doi:10.1126/science.1128214

8. S. W. Ding, O. Voinnet, Antiviral immunity directed by small RNAs. *Cell* **130**, 413–426 (2007). Medline doi:10.1016/j.cell.2007.07.039

9. X. B. Wang, J. Jovel, P. Udomporn, Y. Wang, Q. Wu, W. X. Li, V. Gasciolli, H. Vaucheret, S. W. Ding, The 21-nucleotide, but not 22-nucleotide, viral secondary small interfering RNAs direct potent antiviral defense by two cooperative Argonautes in *Arabidopsis thaliana*. *Plant Cell* **23**, 1625–1638 (2011). Medline doi:10.1105/tpc.110.082305

10. V. N. Kim, J. Han, M. C. Siomi, Biogenesis of small RNAs in animals. *Nat. Rev. Mol. Cell Biol.* **10**, 126–139 (2009). Medline doi:10.1038/nrm2632

11. E. P. Murchison, J. F. Partridge, O. H. Tam, S. Cheloufi, G. J. Hannon, Characterization of Dicer-deficient murine embryonic stem cells. *Proc. Natl. Acad. Sci. U.S.A.* **102**, 12135–12140 (2005). Medline doi:10.1073/pnas.0505479102

12. H. Su, M. I. Trombly, J. Chen, X. Wang, Essential and overlapping functions for mammalian Argonautes in microRNA silencing. *Genes Dev.* **23**, 304–317 (2009). Medline doi:10.1101/gad.1749809

13. P. J. Paddison, A. A. Caudy, G. J. Hannon, Stable suppression of gene expression by RNAi in mammalian cells. *Proc. Natl. Acad. Sci. U.S.A.* **99**, 1443–1448 (2002). Medline doi:10.1073/pnas.032652399

14. E. Billy, V. Brondani, H. D. Zhang, U. Müller, W. Filipowicz, Specific interference with gene expression induced by long, double-stranded RNA in mouse embryonal teratocarcinoma cell lines. *Proc. Natl. Acad. Sci. U.S.A.* **98**, 14428–14433 (2001). Medline doi:10.1073/pnas.261562698

15. J. E. Babiarz, J. G. Ruby, Y. Wang, D. P. Bartel, R. Blelloch, Mouse ES cells express endogenous shRNAs, siRNAs, and other Microprocessor-independent, Dicer-dependent small RNAs. *Genes Dev.* **22**, 2773–2785 (2008). Medline doi:10.1101/gad.1705308

16. F. Weber, V. Wagner, S. B. Rasmussen, R. Hartmann, S. R. Paludan, Double-stranded RNA is produced by positive-strand RNA viruses and DNA viruses but not in detectable amounts by negative-strand RNA viruses. *J. Virol.* **80**, 5059–5064 (2006). Medline doi:10.1128/JVI.80.10.5059-5064.2006

17. Y. Tay, J. Zhang, A. M. Thomson, B. Lim, I. Rigoutsos, MicroRNAs to *Nanog*, *Oct4* and *Sox2* coding regions modulate embryonic stem cell differentiation. *Nature* **455**, 1124–1128 (2008). Medline doi:10.1038/nature07299

18. S. Pfeffer, A. Sewer, M. Lagos-Quintana, R. Sheridan, C. Sander, F. A. Grässer, L. F. van Dyk, C. K. Ho, S. Shuman, M. Chien, J. J. Russo, J. Ju, G. Randall, B. D. Lindenbach, C. M. Rice, V. Simon, D. D. Ho, M. Zavolan, T. Tuschl, Identification of microRNAs of the herpesvirus family. *Nat. Methods* **2**, 269–276 (2005). Medline doi:10.1038/nmeth746

19. E. Allen, Z. Xie, A. M. Gustafson, J. C. Carrington, microRNA-directed phasing during trans-acting siRNA biogenesis in plants. *Cell* **121**, 207–221 (2005). Medline doi:10.1016/j.cell.2005.04.004

20. E. Ma, I. J. MacRae, J. F. Kirsch, J. A. Doudna, Autoinhibition of human dicer by its internal helicase domain. *J. Mol. Biol.* **380**, 237–243 (2008). Medline doi:10.1016/j.jmb.2008.05.005

21. J. A. Diaz-Pendon, F. Li, W. X. Li, S. W. Ding, Suppression of antiviral silencing by cucumber mosaic virus 2b protein in *Arabidopsis* is associated with drastically reduced accumulation of three classes of viral small interfering RNAs. *Plant Cell* **19**, 2053–2063 (2007). Medline doi:10.1105/tpc.106.047449

22. C. S. Sullivan, D. Ganem, A virus-encoded inhibitor that blocks RNA interference in mammalian cells. *J. Virol.* **79**, 7371–7379 (2005). Medline doi:10.1128/JVI.79.12.7371-7379.2005

23. Y. Li, J. Lu, Y. Han, X. Fan, S.-W. Ding, RNA interference functions as an antiviral immunity mechanism in mammals. *Science* **342**, 231 (2013). doi:10.1126/science.1241911

24. J. A. Chao, J. H. Lee, B. R. Chapados, E. W. Debler, A. Schneemann, J. R. Williamson, Dual modes of RNA-silencing suppression by Flock House virus protein B2. *Nat. Struct. Mol. Biol.* **12**, 952–957 (2005). Medline doi:10.1038/nsmb1005

25. X. H. Wang, R. Aliyari, W. X. Li, H. W. Li, K. Kim, R. Carthew, P. Atkinson, S. W. Ding, RNA interference directs innate immunity against viruses in adult *Drosophila*. *Science* **312**, 452–454 (2006). Medline doi:10.1126/science.1125694

26. C. E. Yi, J. M. Bekker, G. Miller, K. L. Hill, R. H. Crosbie, Specific and potent RNA interference in terminally differentiated myotubes. *J. Biol. Chem.* **278**, 934–939 (2003). Medline doi:10.1074/jbc.M205946200

27. L. Gan, K. E. Anton, B. A. Masterson, V. A. Vincent, S. Ye, M. Gonzalez-Zulueta, Specific interference with gene expression and gene function mediated by long dsRNA in neural cells. *J. Neurosci. Methods* **121**, 151–157 (2002). Medline doi:10.1016/S0165-0270(02)00230-3

28. G. D. Penny, G. F. Kay, S. A. Sheardown, S. Rastan, N. Brockdorff, Requirement for *Xist* in X chromosome inactivation. *Nature* **379**, 131–137 (1996). Medline doi:10.1038/379131a0

29. J. Selfridge, A. M. Pow, J. McWhir, T. M. Magin, D. W. Melton, Gene targeting using a mouse HPRT minigene/HPRT-deficient embryonic stem cell system: Inactivation of the mouse *ERCC-1* gene. *Somat. Cell Mol. Genet.* **18**, 325–336 (1992). Medline doi:10.1007/BF01235756

30. C. Ciaudo, F. Jay, I. Okamoto, C.-J. Chen, A. Sarazin , N. Servant, E. Barillot , E. Heard, O. Voinnet, RNAi-dependent and independent control of LINE1 accumulation and mobility in mouse embryonic stem cells. *PLoS Genet.* **9**, e1003791 (2013) doi:10.1371/journal.pgen.1003791.

31. M. Hooper, K. Hardy, A. Handyside, S. Hunter, M. Monk, HPRT-deficient (Lesch-Nyhan) mouse embryos derived from germline colonization by cultured cells. *Nature* **326**, 292–295 (1987). Medline doi:10.1038/326292a0

32. G. Meister, M. Landthaler, A. Patkaniowska, Y. Dorsett, G. Teng, T. Tuschl, Human Argonaute2 mediates RNA cleavage targeted by miRNAs and siRNAs. *Mol. Cell* **15**, 185–197 (2004). Medline doi:10.1016/j.molcel.2004.07.007

33. H. Su, M. I. Trombly, J. Chen, X. Wang, Essential and overlapping functions for mammalian Argonautes in microRNA silencing. *Genes Dev.* **23**, 304–317 (2009). doi:10.1101/gad.1749809 Medline

34. S. Hammoumi, C. Cruciere, M. Guy, A. Boutrouille, S. Messiaen, S. Lecollinet, L. Bakkali-Kassimi, Characterization of a recombinant encephalomyocarditis virus expressing the enhanced green fluorescent protein. *Arch. Virol.* **151**, 1783–1796 (2006). Medline doi:10.1007/s00705-006-0746-7

35. C. J. Chen, N. Servant, J. Toedling, A. Sarazin, A. Marchais, E. Duvernois-Berthet, V. Cognat, V. Colot, O. Voinnet, E. Heard, C. Ciaudo, E. Barillot, ncPRO-seq: A tool for annotation and profiling of ncRNAs in sRNA-seq data. *Bioinformatics* **28**, 3147–3149 (2012). Medline doi:10.1093/bioinformatics/bts587

36. B. Langmead, C. Trapnell, M. Pop, S. L. Salzberg, Ultrafast and memory-efficient alignment of short DNA sequences to the human genome. *Genome Biol.* **10**, R25 (2009). Medline doi:10.1186/gb-2009-10-3-r25

37. R Development Core Team, *R: A Language and Environment for Statistical Computing* (R Foundation for Statistical Computing, Vienna, 2011).

38. H. Hassani, Singular spectrum analysis: Methodology and comparison. *J. Data Sci.* **5**, 239–257 (2007).

39. A. Korobeynikov, Computation- and space-efficient implementation of SSA. *Statist. Its Interface* **3**, 357–368 (2010). doi:10.4310/SII.2010.v3.n3.a9

40. J. Sambrook, D. Russell, *Molecular Cloning: A Laboratory Manual* (Cold Spring Harbor Laboratory Press, Cold Spring Harbor, New York, ed. 3, 2001).

41. P. Dunoyer, C. Himber, V. Ruiz-Ferrer, A. Alioua, O. Voinnet, Intra- and intercellular RNA interference in *Arabidopsis thaliana* requires components of the microRNA and heterochromatic silencing pathways. *Nat. Genet.* **39**, 848–856 (2007). Medline doi:10.1038/ng2081

42. F. Jay, C. Ciaudo, An RNA tool kit to study the status of mouse ES cells: Sex determination and stemness. *Methods* **63**, 85–92 (2013).

43. G. S. Pall, A. J. Hamilton, Improved northern blot method for enhanced detection of small RNA. *Nat. Protoc.* **3**, 1077–1084 (2008). Medline doi:10.1038/nprot.2008.67

44. C. Ciaudo, A. Bourdet, M. Cohen-Tannoudji, H. C. Dietz, C. Rougeulle, P. Avner, Nuclear mRNA degradation pathway(s) are implicated in *Xist* regulation and X chromosome inactivation. *PLoS Genet.* **2**, e94 (2006). Medline doi:10.1371/journal.pgen.0020094

45. E. V. Pilipenko, V. M. Blinov, B. K. Chernov, T. M. Dmitrieva, V. I. Agol, Conservation of the secondary structure elements of the 5′-untranslated region of cardio- and aphthovirus RNAs. *Nucleic Acids Res.* **17**, 5701–5711 (1989). Medline doi:10.1093/nar/17.14.5701

46. V. G. Kolupaeva, I. B. Lomakin, T. V. Pestova, C. U. Hellen, Eukaryotic initiation factors 4G and 4A mediate conformational changes downstream of the initiation codon of the encephalomyocarditis virus internal ribosomal entry site. *Mol. Cell. Biol.* **23**, 687–698 (2003). Medline doi:10.1128/MCB.23.2.687-698.2003

47. K. Darty, A. Denise, Y. Ponty, VARNA: Interactive drawing and editing of the RNA secondary structure. *Bioinformatics* **25**, 1974–1975 (2009). Medline doi:10.1093/bioinformatics/btp250

48. R. Lorenz, S. H. Bernhart, C. Höner Zu Siederdissen, H. Tafer, C. Flamm, P. F. Stadler, I. L. Hofacker, ViennaRNA Package 2.0. *Algorithms Mol. Biol.* **6**, 26 (2011). Medline doi:10.1186/1748-7188-6-26